Supplement of

Molecular evolution of oxygenated organic molecules in a cloud-influenced forested mountain environment

Yi Zhang et al.

Correspondence to: Yele Sun (sunyele@mail.iap.ac.cn)

Text S1. Semi-quantitative calibration of I-CIMS

The calibration of I-CIMS is challenging because most OOMs are highly reactive and often possess low vapor pressures, making the preparation of stable calibration standards difficult. Therefore, a semi-quantitative calibration approach widely adopted in previous I-CIMS studies was applied to estimate OOM mixing ratios (Isaacman-Vanwertz et al., 2018; Lopez-Hilfiker et al., 2016).

The conversion from measured ion signal intensity to mixing ratio can be expressed as:

$$\text{Mixing Ratio}_i = \frac{\text{Signal}_i}{S_{max} \times (1/S_0)_i \times \text{RTE}_i}$$

where S_{max} represents the maximum achievable sensitivity among all detected compounds. Previous studies have shown that the iodide adduct of levoglucosan approaches the collision limit and therefore exhibits the highest sensitivity and transmission efficiency in iodide-CIMS measurements (Lopez-Hilfiker et al., 2016; Iyer et al., 2016). The term $(1/S_0)_i$ accounts for compound-dependent variations in sensitivity caused by differences in iodide-adduct stability. This parameter is closely related to the binding energy between the analyte molecule and the iodide reagent ion. Following the method of Lopez-Hilfiker et al. (2016), voltage-scanning experiments were performed by varying the voltage difference (ΔV) between the skimmer and the entrance to the second quadrupole. For each iodide-adduct ion, the remaining signal fraction relative to the maximum signal was fitted using a sigmoidal function, yielding two characteristic parameters: $1/S_0$, defined as the ratio of the signal at $\Delta V = 2.5$ V to the maximum signal, and dV_{50}, defined as the voltage at which the signal decreases to half of its maximum value. The empirical relationship between $1/S_0$ and dV_{50} is given by:

$$\frac{1}{S_0} = 0.49 + \frac{0.49}{1 + \exp\left(\frac{0.014 - dV_{50}}{0.39}\right)}$$

The relative transmission efficiency (RTE_i) accounts for mass-dependent ion transmission through the instrument optics. It was calibrated using a suite of perfluorinated carboxylic acids that form stable iodide-adduct clusters. The resulting transmission efficiency curve was parameterized as a Gaussian function of *m/z*:

$$\text{RTE}_i = 0.29 + 0.89 * \exp\left(-\left(\frac{m/z - 279.74}{231.24}\right)^2\right)$$

The parameterization employed in the semi-quantitative calibration procedure followed that reported by Zhang et al. (2026b). This semi-quantitative approach has been extensively applied in previous field studies (Li et al., 2026; Ye et al., 2021) and provides reasonable estimates of OOM mixing ratios in the absence of authentic calibration standards for individual compounds.

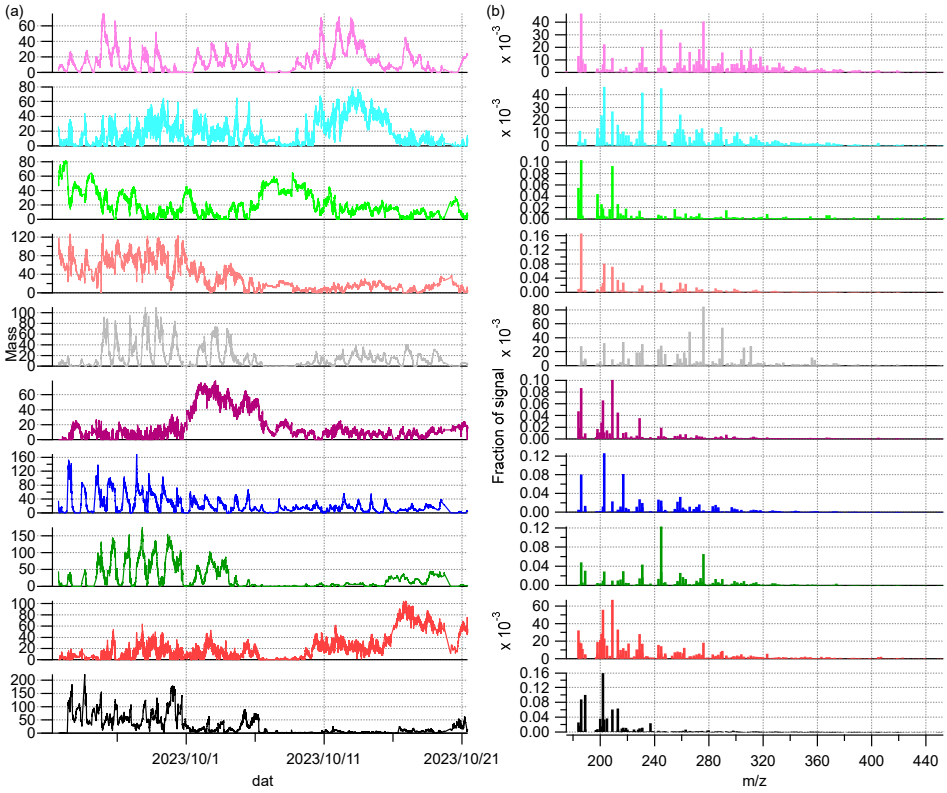

Figure TS1: (a) Time series and (b) mass profiles of PMF ten-factor solution.

Text S2. PMF data preparation and diagnosis

The PMF input consisted of the concentration matrix and the corresponding uncertainty matrix of the detected OOM species. The calculation of the uncertainty matrix (**Unc**) is described as follows:

$$\mathbf{Unc} = \begin{cases} \frac{5}{6} \times \mathrm{MDL_i}, c_i \leq \mathrm{MDL_i} \\ \sqrt{(\mathrm{Ef} \times c_i)^2 + (0.5 \times \mathrm{MDL_i})^2}, c_i > \mathrm{MDL_i} \end{cases}$$

where MDL_i represents the detection limit of i^{th} species, c_i represents the mixing ratio of i^{th} species, and the error fraction (Ef) is set to 20% in this study.

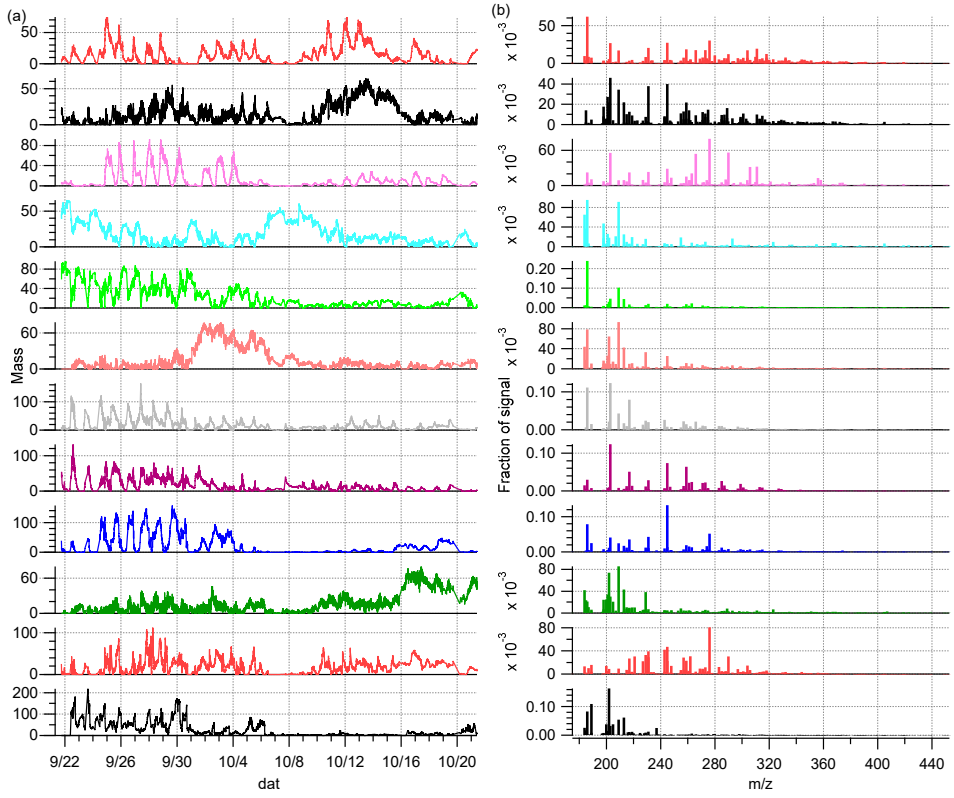

Figure TS2: (a) Time series and (b) mass profiles of PMF twelve-factor solution.

To determine the optimal factor solution, PMF was performed using solutions ranging from 3 to 14 factors. The resulting solutions were evaluated comprehensively based on (1) the variation of the Q/Q_{exp} value, (2) the chemical interpretability of factor profiles, (3) the temporal evolution of factor time series, (4) the physical significance of the diurnal patterns, and (5) the presence of characteristic molecular tracers associated with known atmospheric sources and oxidation pathways. After comparison of the candidate solutions, the eleven-factor solution was selected as the optimal representation of the dataset. In the ten-factor solution, the Forenoon ISO+MT oxidation factor could not be resolved as an independent factor and was merged with other biogenic oxidation sources (Fig. TS1). In contrast, the twelve-factor solution produced an additional factor lacking clear chemical characteristics and physical interpretability, indicating over-resolution of the dataset (Fig. TS2). Furthermore,

the decrease in Q/Q_{exp} beyond the eleven-factor solution was negligible (relative variation smaller than 4.2%, Fig. TS3), suggesting limited improvement in model performance. Therefore, the eleven-factor solution was considered the most robust and physically meaningful representation of the observed OOM dataset. Among the eleven resolved factors, nine were identified as atmospherically relevant factors and were assigned to specific sources or oxidation processes based on their characteristic molecular compositions, temporal behaviour, and relationships with external tracers. These factors were designated as Daytime ISO oxidation, Forenoon ISO+MT oxidation, Afternoon ISO oxidation, Afternoon ISO+MT oxidation, Nighttime ISO+MT oxidation, Nitrogen-containing species, Sulfur-containing species, Anthropogenic organic nitrates, and Regional transport. The remaining two factors (BG1 and BG2) were characterized primarily by instrumental background signals (Fig. TS4). Because these factors lacked meaningful atmospheric signatures and were not associated with identifiable sources or chemical processes, they were excluded from subsequent source apportionment and discussion.

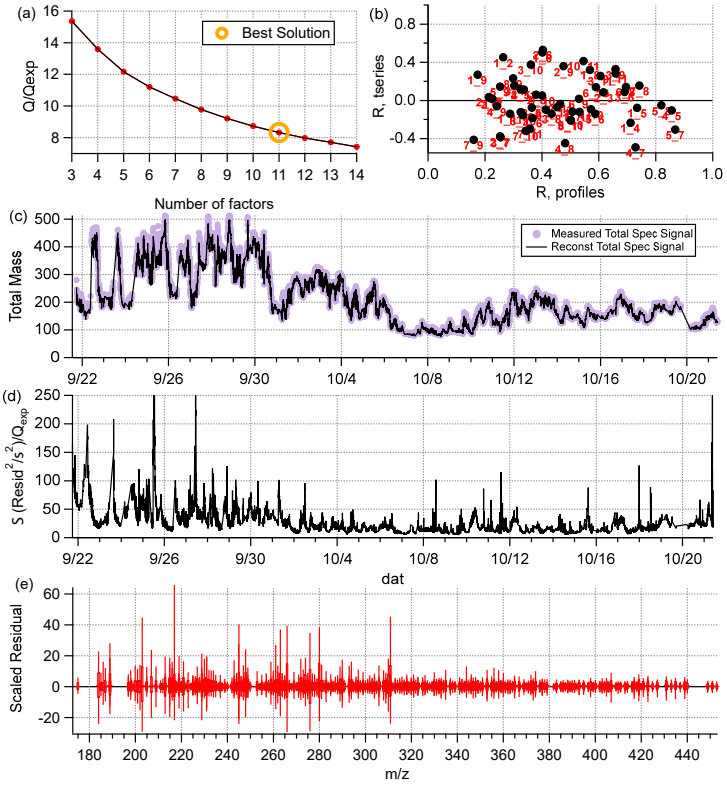

Figure TS3: Diagnostic plots of the PMF results (eleven solution).

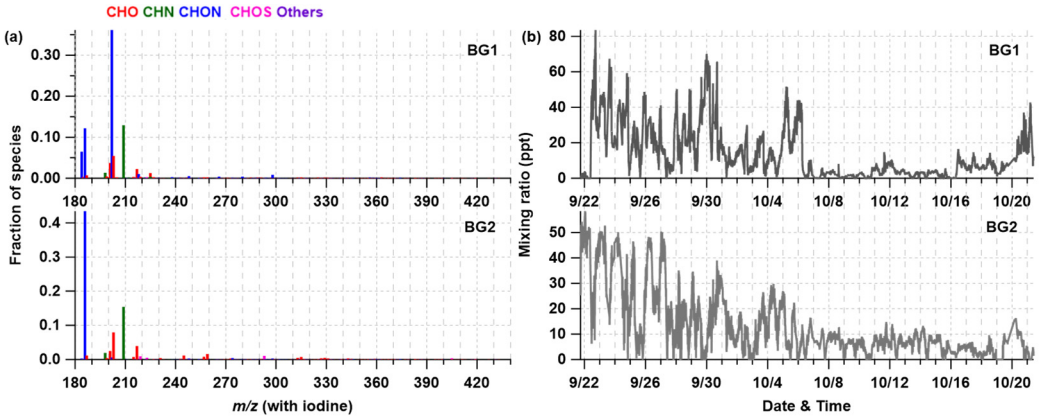

Figure TS4: (a) The mass profiles and (b) time series of the two artifact factors.

Text S3. Estimation of OH radical concentrations

The concentration of OH radicals was estimated using a steady-state approach. Under the assumption that the atmospheric production and loss rates of OH radicals are balanced, the steady-state OH concentration can be expressed as:

$$[\mathrm{OH}]_{\mathrm{SS}} = \frac{\alpha k_{O_3+alkene}[\mathrm{O_3}][\mathrm{alkene}]}{k_{OH+alkene}[\mathrm{alkene}] + k_{OH+O_3}[\mathrm{O_3}]}$$

where $k_{O_3+alkene}$ denotes the rate constant for the reaction of ozone with unsaturated VOCs, α represents the OH radical yield from ozonolysis, $k_{OH+alkene}$ is the rate constant for the reaction of OH radicals with alkene, and k_{OH+O_3} is the rate constant for the reaction between OH radicals and ozone, were obtained from Atkinson et al. (1992). At the SH site, isoprene and monoterpenes were identified as the dominant reactive biogenic alkenes and were therefore assumed to represent the major VOC sinks and sources relevant to OH production through ozonolysis (Zhang et al., 2024). The rate constants for the reactions of ozone with isoprene and monoterpenes were taken from Khamaganov and Hites (2001), while the corresponding OH yields were adopted from Nguyen et al. (2016) for isoprene and Rickard et al. (1999) for monoterpenes. Using the observed concentrations of isoprene, monoterpenes, and ozone, the steady-state OH concentration was calculated for the entire observation period. The average ozone concentration across the four periods was 48.8 ± 8.5 ppb (mean ± standard deviation). Based on the steady-state calculation, the mean OH concentration was estimated to be 0.074 ± 0.01 ppt (1.6×10^6 molecules cm^{-3}). It should be noted that this approach provides a first-order estimate of ambient OH levels and does not explicitly account for additional OH sources and sinks, such as photolysis reactions, heterogeneous processes, or radical

recycling mechanisms. Nevertheless, the calculated OH concentration falls within the range reported for remote and forested environments and is sufficient for evaluating the relative importance of OH-initiated oxidation pathways in this study.

Text S4. Estimation of NO_3 radical concentrations

The concentration of NO_3 radicals was estimated using a steady-state approximation. Assuming that the atmospheric production and loss rates of NO_3 radicals are balanced, the steady-state concentration of NO_3 can be expressed as:

$$[NO_3]_{SS} = \frac{k_{O_3+NO_2}[O_3][NO_2]}{k_{NO_3+MT}[MT] + k_{NO_3+ISO}[ISO]}$$

where $k_{O_3+NO_2}$ represents the rate coefficient for the formation of NO_3 radicals through the reaction of ozone with NO_2. The temperature-dependent rate coefficient was calculated using the parameterization recommended by previous kinetic studies (Vrekoussis et al., 2004). k_{NO_3+MT} and k_{NO_3+ISO} denote the reaction rate constants of NO_3 radicals with monoterpenes and isoprene, respectively, and were taken from Peräkylä et al. (2014). The observed concentrations of ozone, NO_2, isoprene, and monoterpenes were used to estimate the production and loss rates of NO_3 radicals throughout the campaign. Based on this approach, the average NO_3 radical concentration during the observation period was estimated to be 0.6 ± 0.2 ppt (mean ± standard deviation). This concentration level is comparable to values previously reported for forested and mountainous regions in southern China (Gong et al., 2018), suggesting that the estimated NO_3 concentrations are reasonable for the study area. It should be noted that the present calculation only considers the dominant production pathway of NO_3 radicals and their losses through reactions with biogenic alkenes. Additional NO_3 sinks, including reactions with nitric oxide (NO), heterogeneous uptake of N_2O_5, and hydrolysis processes, were not explicitly included in the calculation. Consequently, the estimated NO_3 concentrations should be regarded as first-order approximations. Nevertheless, the resulting values are consistent with previous observations in similar environments and are therefore considered suitable for evaluating the relative importance of NO_3-initiated oxidation pathways in the formation of OOMs and organic nitrates during the campaign.

Text S5. Estimation of the relative importance of OH- and O_3-initiated oxidation

To evaluate the relative importance of OH radicals and O_3 in the oxidation of biogenic volatile organic compounds (BVOCs), the oxidation rates of isoprene and monoterpenes were estimated using a kinetic approach. The oxidation rates of isoprene by OH radicals and O_3 were calculated as:

$$R_{ISO+OH} = k_{ISO+OH}[ISO][OH]$$

$$R_{ISO+O_3} = k_{ISO+OH}[ISO][O_3]$$

where k represents the bimolecular reaction rate coefficient, and [ISO], [OH], and [O_3] denote the concentrations of isoprene, OH radicals, and ozone, respectively. The reaction rate coefficients were taken from (Zhang et al., 2000; Khamaganov and Hites, 2001). OH radical concentrations were estimated using the photochemical steady-state approach described in Text S3, yielding an average concentration of 0.074 (± 0.01) ppt, 1.6×10^6 molecules cm^{-3}, across the four periods. Ozone concentrations were approximately 45 ppb at 09:00 and 50 ppb at 20:00. Using these values, the oxidation rates of isoprene by OH radicals and O_3 were estimated. The calculated oxidation rate of isoprene by OH radicals was approximately 15 times greater than that by O_3, indicating that OH oxidation dominated isoprene processing at the SH site.

The same approach was applied to monoterpenes:

$$R_{MT+OH} = k_{MT+OH}[ISO][OH]$$

$$R_{MT+O_3} = k_{MT+OH}[ISO][O_3]$$

where the reaction rate coefficients were obtained from Atkinson et al. (1986) and Stewart et al. (2013). The calculated oxidation rate of monoterpenes by OH radicals was approximately 1.5 times that by O_3, suggesting that both OH-initiated oxidation and ozonolysis contributed substantially to monoterpene oxidation under ambient conditions.

Text S6. Estimation of the relative contributions of NO_3-initiated oxidation to ON formation

To evaluate the relative importance of O_3- and NO_3-initiated oxidation pathways in the formation of biogenic ONs, the oxidation rates of isoprene and monoterpenes were estimated using:

$$R_{ISO+NO_3} = k_{ISO+NO_3}[ISO][NO_3]$$

$$R_{MT+NO_3} = k_{MT+NO_3}[ISO][NO_3]$$

where k denotes the bimolecular reaction rate coefficient and $[NO_3]$ represents the concentration of NO_3 radicals. The NO_3 radical concentration was estimated using the steady-state approach described in Text S4, yielding an average concentration of 0.6 (± 0.2) ppt during the observation period. Reaction rate coefficients were adopted from Peräkylä et al. (2014). Although the reaction rate coefficient of isoprene with NO_3 radicals is approximately four orders of magnitude larger than that with O_3, ambient O_3 concentrations were approximately 8.6×10^4 times higher than NO_3 radical concentrations.

Consequently, the estimated oxidation rate of isoprene by O_3 was approximately 8.6 times higher than that by NO_3 radicals, indicating that ozonolysis represents an important pathway contributing to ISO-ON formation. In contrast, monoterpenes reacted much more rapidly with NO_3 radicals. Based on the observed precursor concentrations and calculated oxidant levels, the oxidation rate of monoterpenes by NO_3 radicals was estimated to be approximately 1.65 times higher than that by O_3. This result suggests that both NO_3-initiated oxidation and ozonolysis contribute substantially to MT-ON formation, with the NO_3 pathway being slightly more important under the conditions observed at the SH site.

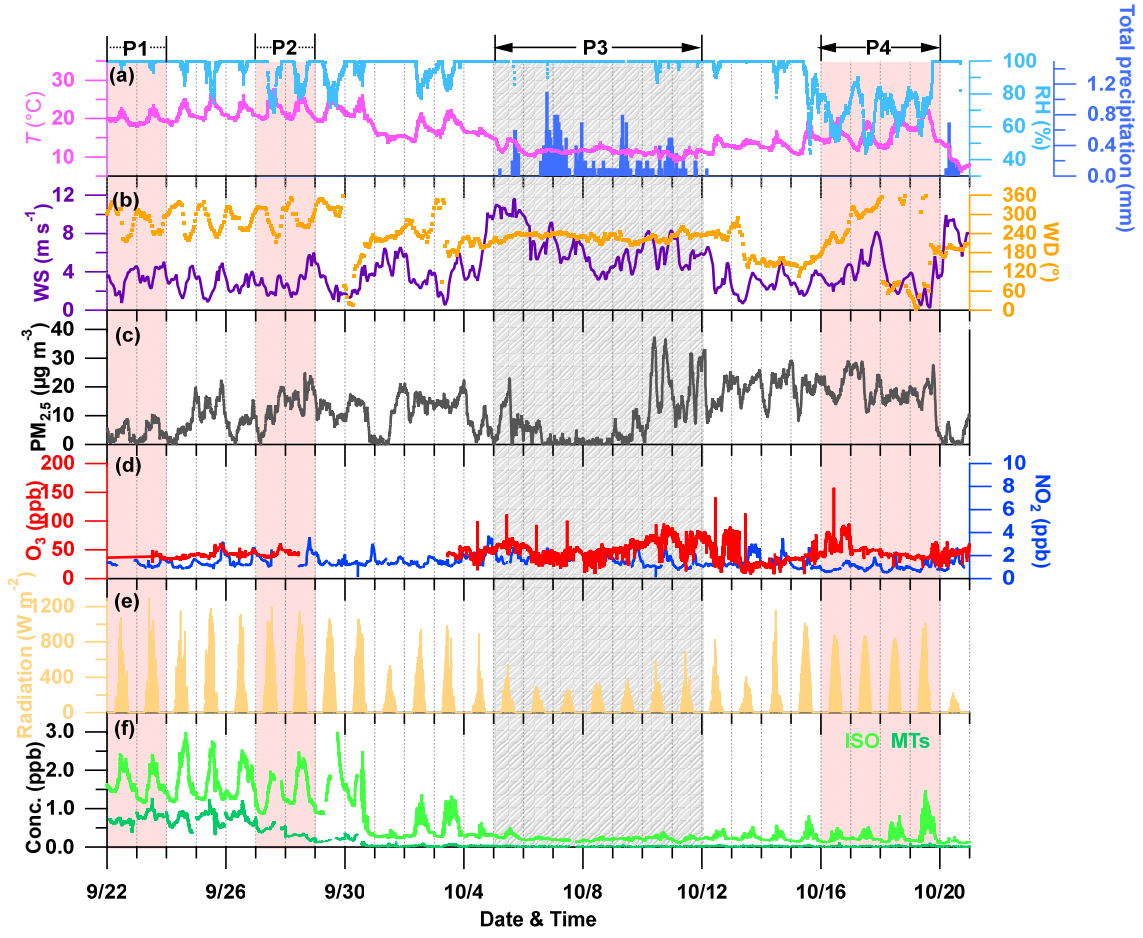

Figure S1: Time series of (a) temperature (*T*), relative humidity (RH), precipitation, (b) wind direction (WD) and wind speed (WS), (c) mass concentration of $PM_{2.5}$, (d) ozone (O_3) and nitrogen dioxide (NO_2) concentration, (e) radiation intensity, (f) isoprene and monoterpenes during the observation period in autumn 2023.

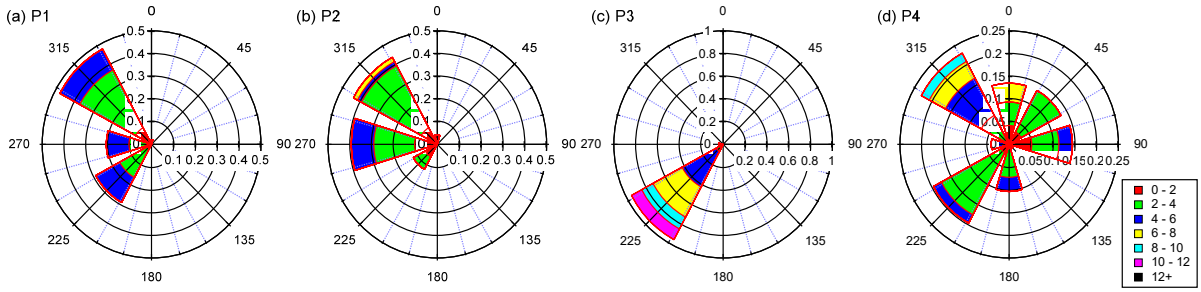

Figure S2: Wind rose diagrams for the four periods.

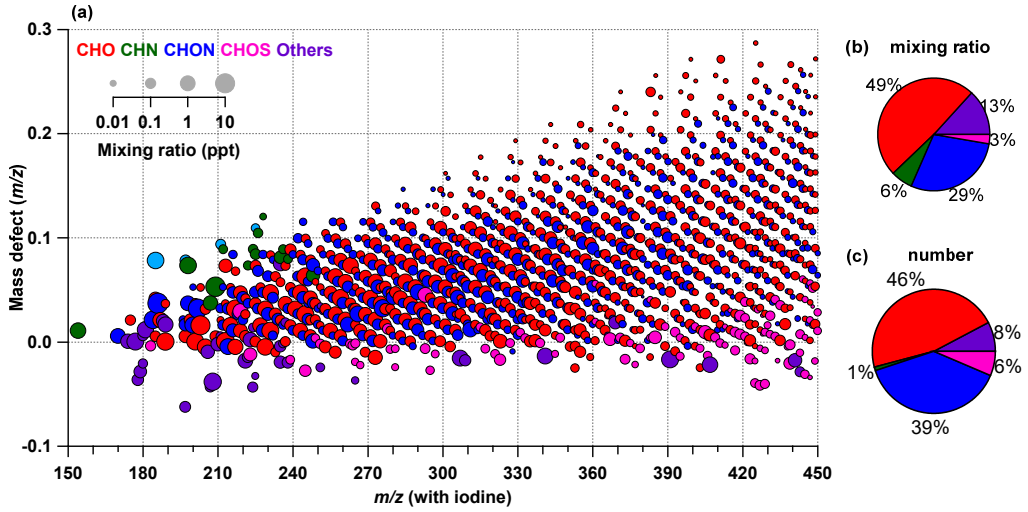

Figure S3: (a) Mass defect plot of the ions detected by I-CIMS during the observation period. The circle colour represents the elemental composition, and the circle size corresponds to the mixing ratio of the ions. (b) Pie chart of ion mixing ratios from different elemental compositions. (c) Pie chart of ion numbers from different elemental compositions.

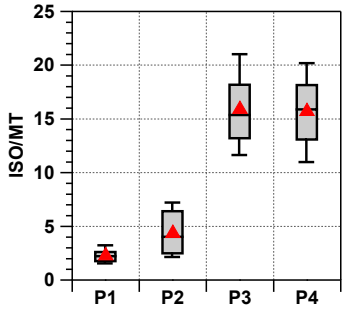

Figure S4: Comparison of the isoprene-to-monoterpene concentration ratios (ISO/MT) among the four periods.

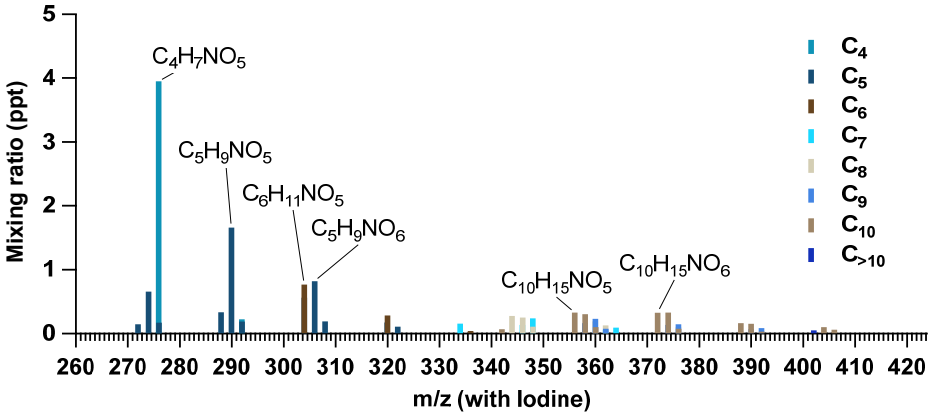

Figure S5: Mass spectrum of organic nitrates measured by I-CIMS coloured by the number of carbon.

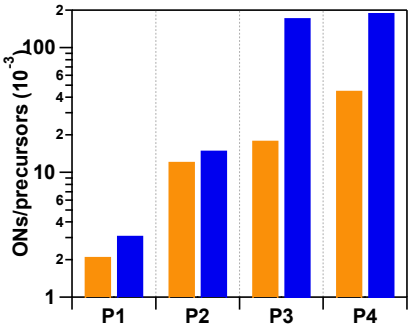

Figure S6: (a) The ratios of ISO-Ons/isoprene and MT-ONs/monoterpenes during the four periods.

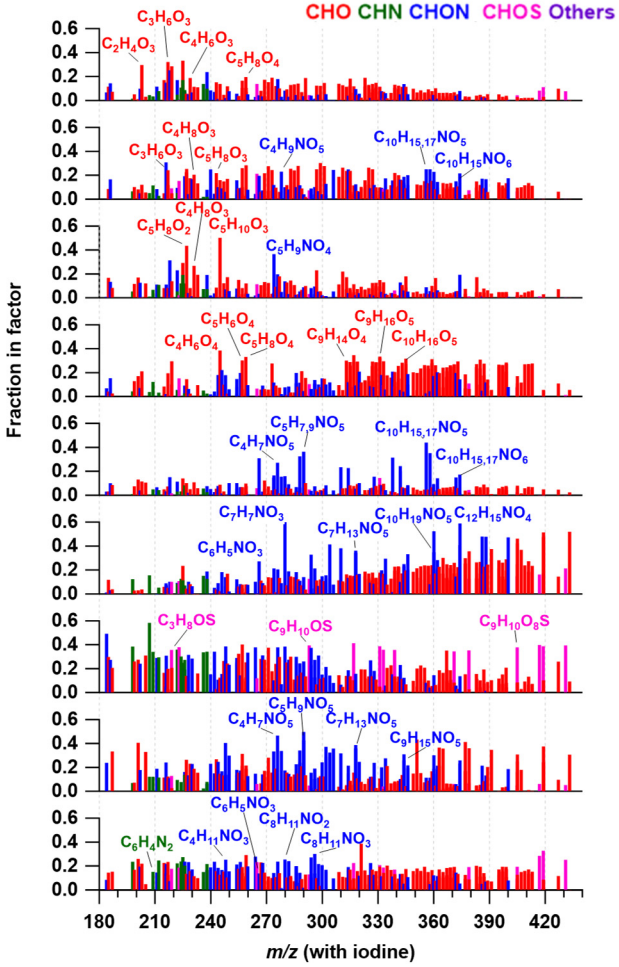

Figure S7: The fractional contribution of each resolved factor for OOM species.

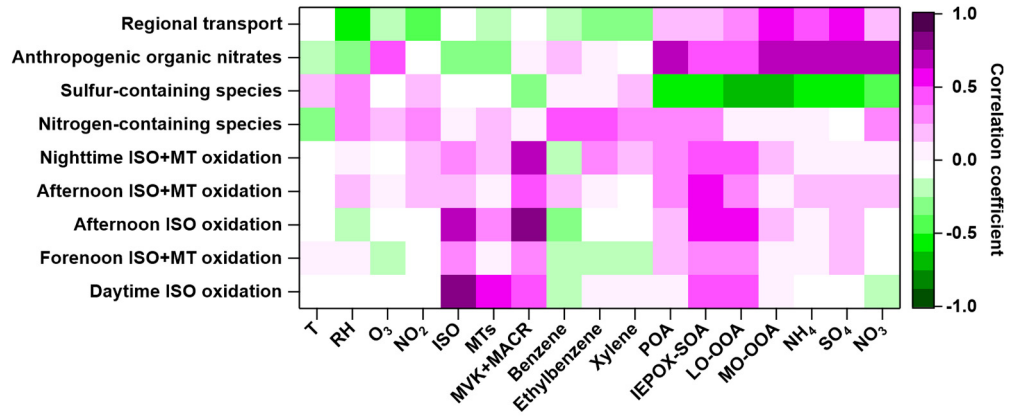

Figure S8: Pearson correlation coefficients between the PMF-resolved OOM factors and selected external tracers.

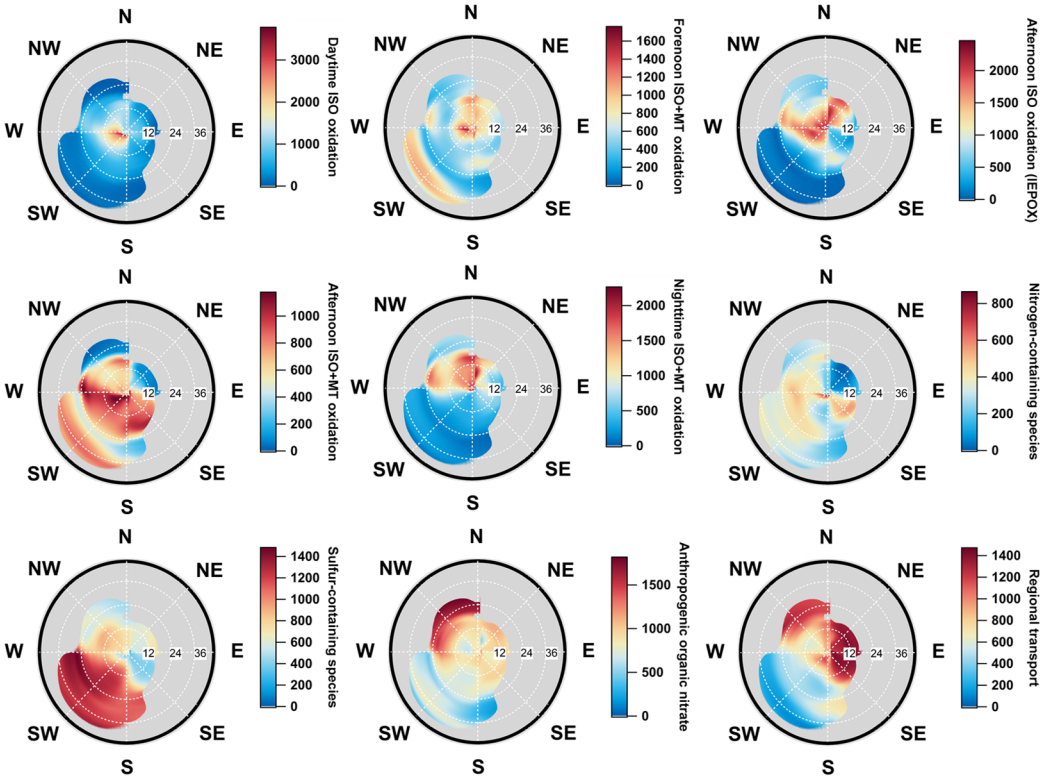

Figure S9: Wind speed- and wind direction-dependent concentration distributions of the PMF-resolved OOM factors derived from non-parametric wind regression (NWR).

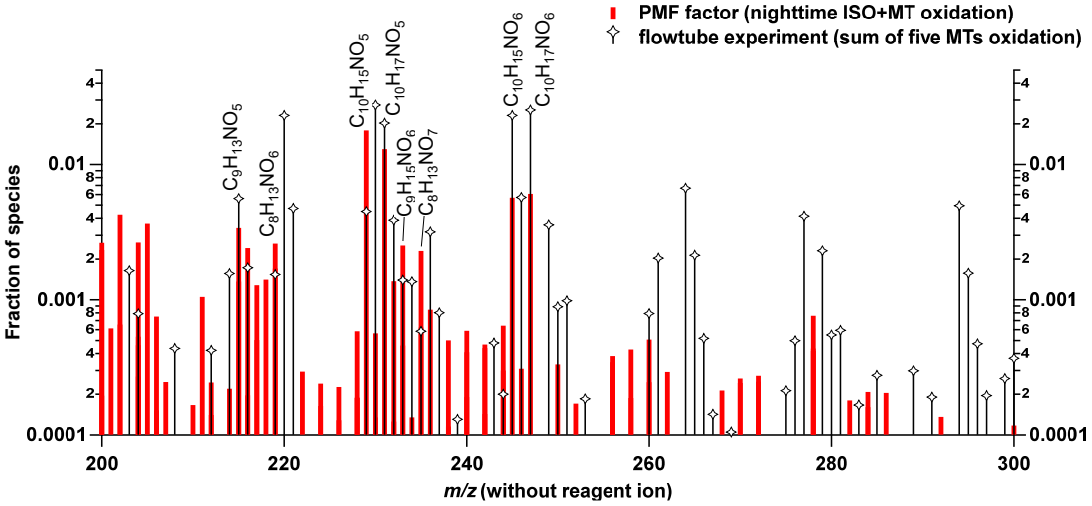

Figure S10: Comparison between the characteristic mass spectrum of the Nighttime ISO+MT oxidation factor and the oxidation products from monoterpenes + NO_3 reactions obtained in flowtube experiments (Zhang et al., 2026a). The reported m/z values represent neutral molecular masses after subtraction of the reagent ion.

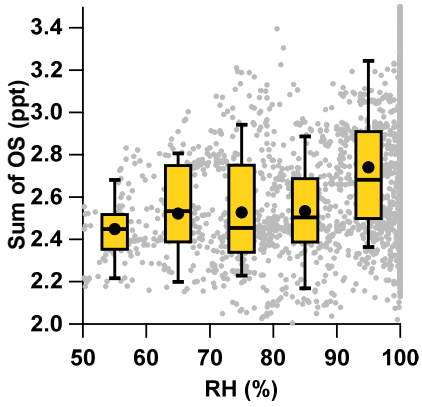

Figure S11: Sum of Sulfur-containing OOMs as a function of RH.

Table S1: Summary of instruments used in autumn observations in 2023, including instrument name, measurement element, model/company, and temporal resolution.

Instrument	Species	Model/Company	Time resolution
I-CIMS	OOMs	TOFWERK	1 s
Vocus PTR-MS	VOCs	TOFWERK	1 s
TOF-ACSM	NR-$PM_{2.5}$	Aerodyne Research Inc.	2 min
AE33	BC	Aerosol Magee Scientific	1 s
GCVI	cloud droplets	Brechtel Manufacturing Inc.	1 s
Gas analyzer	O_3	Model 49i, Thermo Scientific Inc.	1 min
Gas analyzer	CO	G2401, Picarro Inc.	1 min
TD-LIF	NO_2	Customed	1 min
Ambient particulate monitor	$PM_{2.5}$	Model 5014i, Thermo Scientific Inc.	1 min
Standard meteo probe	RH, *T*	HC2S3, Campbell Scientific Inc.	1 min

Table S2: Comparison of meteorological parameters and trace gas concentrations among the four periods.

Parameter	P1	P2	P3	P4
T (°C)	19.8±1.1	22.4±2.1	11.5±1.0	16.4±2.7
RH (%)	99.8±0.7	93.2±8.9	99.8±1.1	72.0±12.0
WS (m s^{-1})	3.35±1.04	2.90±1.22	6.58±2.11	3.58±1.77
WD (°)	279.7±35.4	288.2±33.3	229.7±10.8	203.8±109.6
$PM_{2.5}$ (μg m^{-3})	4.22±2.71	13.34±5.68	7.86±9.04	18.70±4.95
Ozone (ppb)	38.0±2.9	43.8±5.0	53.3±14.7	48.7±13.4
NO_2 (ppb)	1.3±0.2	1.7±0.6	1.6±0.4	1.0±0.3
Radiation (W m^{-2})	141.3±203.2	206.2±298.4	63.3±92.1	213.3±301.7
Isoprene (ppb)	1.64±0.31	1.41±0.42	0.22±0.05	0.27±0.17
Monoterpene (ppb)	0.75±0.13	0.36±0.12	0.01±0.00	0.02±0.01

References

Atkinson, R., Aschmann, S. M., and Pitts Jr, J. N.: Rate constants for the gas-phase reactions of the OH radical with a series of monoterpenes at 294 ± 1 K, Int. J. Chem. Kinet., 18, 287-299, 10.1002/kin.550180303, 1986.

Atkinson, R., Baulch, D. L., Cox, R. A., Hampson, R. F., Kerr, J. A., and Troe, J.: Evaluated kinetic and photochemical data for atmospheric chemistry: Supplement IV: IUPAC subcommittee on gas kinetic data evaluation for atmospheric chemistry, Atmos. Environ., Part A, 26, 1187-1230, 10.1016/0960-1686(92)90383-V, 1992.

Gong, D., Wang, H., Zhang, S., Wang, Y., Liu, S. C., Guo, H., Shao, M., He, C., Chen, D., He, L., Zhou, L., Morawska, L., Zhang, Y., and Wang, B.: Low-level summertime isoprene observed at a forested mountaintop site in southern China: implications for strong regional atmospheric oxidative capacity, Atmos. Chem. Phys., 18, 14417-14432, 10.5194/acp-18-14417-2018, 2018.

Isaacman-VanWertz, G., Massoli, P., O'Brien, R., Lim, C., Franklin, J. P., Moss, J. A., Hunter, J. F., Nowak, J. B., Canagaratna, M. R., Misztal, P. K., Arata, C., Roscioli, J. R., Herndon, S. T., Onasch, T. B., Lambe, A. T., Jayne, J. T., Su, L., Knopf, D. A., Goldstein, A. H., Worsnop, D. R., and Kroll, J. H.: Chemical evolution of atmospheric organic carbon over multiple generations of oxidation, Nat. Chem., 10, 462-468, 10.1038/s41557-018-0002-2, 2018.

Iyer, S., Lopez-Hilfiker, F., Lee, B. H., Thornton, J. A., and Kurtén, T.: Modeling the detection of organic and inorganic compounds using iodide-based chemical ionization, J. Phys. Chem. A, 120, 576-587, 10.1021/acs.jpca.5b09837, 2016.

Khamaganov, V. G. and Hites, R. A.: Rate Constants for the Gas-Phase Reactions of Ozone with Isoprene, α- and β-Pinene, and Limonene as a Function of Temperature, J. Phys. Chem. A, 105, 815-822, 10.1021/JP002730Z, 2001.

Li, Y., Zhou, W., Sun, J., Lei, L., Xu, W., Zhang, Z., Zhang, Y., Du, A., Ye, P., Wang, J., Aruffo, E., Wang, Z., Worsnop, D. R., and Sun, Y.: Oxygenated organic molecules in urban Beijing: Contrasting summer–winter composition, sources, and roles in secondary organic aerosol formation, Environ. Sci. Technol., 60, 4990-5004, 10.1021/acs.est.5c17177, 2026.

Lopez-Hilfiker, F. D., Iyer, S., Mohr, C., Lee, B. H., D'Ambro, E. L., Kurtén, T., and Thornton, J. A.: Constraining the sensitivity of iodide adduct chemical ionization mass spectrometry to multifunctional organic molecules using the collision limit and thermodynamic stability of iodide ion adducts, Atmos. Meas. Tech., 9, 1505-1512, 10.5194/amt-9-1505-2016, 2016.

Nguyen, T. B., Tyndall, G. S., Crounse, J. D., Teng, A. P., Bates, K. H., Schwantes, R. H., Coggon, M. M., Zhang, L., Feiner, P., Millller, D. O., Skog, K. M., Rivera-Rios, J. C., Dorris, M., Olson, K. F., Koss, A., Wild, R. J., Brown, S. S., Goldstein, A. H., de Gouw, J. A., Brune, W. H., Keutsch, F. N., Seinfeld, J. H., and Wennberg, P. O.: Atmospheric fates of Criegee intermediates in the ozonolysis of isoprene, Phys. Chem. Chem. Phys., 18, 10241-10254, 10.1039/C6CP00053C, 2016.

Peräkylä, O., Vogt, M., Tikkanen, O.-P., Laurila, T., Kajos, M. K., Rantala, P. A., Patokoski, J., Aalto, J., Yli-Juuti, T., Ehn, M., Sipila, M., Paasonen, P., Rissanen, M., Nieminen, T., Taipale, R., Keronen, P., Lappalainen, H. K., Ruuskanen, T. M., Rinne, J., Kerminen, V.-M., Kulmala, M., Back, J., and Petaja, T.: Monoterpenes' oxidation capacity and rate over a

boreal forest : temporal variation and connection to growth of newly formed particles, Boreal Environ. Res., 19, 293–310, 2014.

Rickard, A. R., Johnson, D., McGill, C. D., and Marston, G.: OH yields in the gas-phase reactions of ozone with alkenes, J. Phys. Chem. A Mol. Spectrosc. Kinet. Environ. Gen. Theory, 103, 7656-7664, 10.1021/jp9916992, 1999.

Stewart, D. J., Almabrok, S. H., Lockhart, J. P., Mohamed, O. M., Nutt, D. R., Pfrang, C., and Marston, G.: The kinetics of the gas-phase reactions of selected monoterpenes and cyclo-alkenes with ozone and the NO3 radical, Atmos. Environ., 70, 227-235, 10.1016/j.atmosenv.2013.01.036, 2013.

Vrekoussis, M., Kanakidou, M., Mihalopoulos, N., Crutzen, P. J., Lelieveld, J., Perner, D., Berresheim, H., and Baboukas, E.: Role of the NO3 radicals in oxidation processes in the eastern Mediterranean troposphere during the MINOS campaign, Atmos. Chem. Phys., 4, 169-182, 10.5194/acp-4-169-2004, 2004.

Ye, C., Yuan, B., Lin, Y., Wang, Z., Hu, W., Li, T., Chen, W., Wu, C., Wang, C., Huang, S., Qi, J., Wang, B., Wang, C., Song, W., Wang, X., Zheng, E., Krechmer, J. E., Ye, P., Zhang, Z., Wang, X., Worsnop, D. R., and Shao, M.: Chemical characterization of oxygenated organic compounds in the gas phase and particle phase using iodide CIMS with FIGAERO in urban air, Atmos. Chem. Phys., 21, 8455-8478, 10.5194/acp-21-8455-2021, 2021.

Zhang, J., Zhang, Y., Koskenvaara, H., Zhao, J., and Ehn, M.: Gas-phase products from nitrate radical oxidation of five monoterpenes: insights from free-jet flow-tube experiments, Atmos. Chem. Phys., 26, 3933-3949, 10.5194/acp-26-3933-2026, 2026a.

Zhang, R., Suh, I., Lei, W., Clinkenbeard, A. D., and North, S. W.: Kinetic studies of OH-initiated reactions of isoprene, J. Geophys. Res. Atmos., 105, 24627-24635, 10.1029/2000JD900330, 2000.

Zhang, Y., Xu, W., Zhou, W., Li, Y., Zhang, Z., Du, A., Qiao, H., Kuang, Y., Liu, L., Zhang, Z., He, X., Cheng, X., Pan, X., Fu, Q., Wang, Z., Ye, P., Worsnop, D. R., and Sun, Y.: Characterization of organic vapors by a Vocus proton-transfer-reaction mass spectrometry at a mountain site in southeastern China, Sci. Total Environ., 919, 170633, 10.1016/j.scitotenv.2024.170633, 2024.

Zhang, Z., Yuan, Q., Wang, J., Jiang, J., Xu, W., Zeng, S., Zhang, Y., Zhou, W., Li, Y., Huang, X., Chen, X., Xia, M., Yan, C., Hu, B., Wang, Z., Li, J., Liu, Y., Kulmala, M., Worsnop, D. R., and Sun, Y.: Oxygenated Organic Molecules Drive Particle Growth and Secondary Organic Aerosol Formation in Beijing Winter, Environ. Sci. Technol. Lett., 13, 713-719, 10.1021/acs.estlett.6c00009, 2026b.